Residual Cone Structure in Patients With X-Linked Cone Opsin Mutations

Emily J. Patterson,[1] Angelos Kalitzeos,[2,3] Melissa Kasilian,[2,3] Jessica C. Gardner,[2,3] Jay Neitz,[4] Alison J. Hardcastle,[2,3] Maureen Neitz,[4] Joseph Carroll,[1,5,6] and Michel Michaelides[2,3]

[1]Department of Ophthalmology and Visual Sciences, Medical College of Wisconsin, Milwaukee, Wisconsin, United States
[2]University College London Institute of Ophthalmology, London, United Kingdom
[3]Moorfields Eye Hospital, London, United Kingdom
[4]Department of Ophthalmology, University of Washington, Seattle, Washington, United States
[5]Department of Biophysics, Medical College of Wisconsin, Milwaukee, Wisconsin, United States
[6]Department of Cell Biology, Neurobiology, and Anatomy, Medical College of Wisconsin, Milwaukee, Wisconsin, United States

Correspondence: Joseph Carroll, Department of Ophthalmology and Visual Sciences, Medical College of Wisconsin, 925 N. 87th Street, Milwaukee, WI 53226, USA; jcarroll@mcw.edu.
Michel Michaelides, University College London Institute of Ophthalmology, 11-43 Bath Street, London EC1V 9EL, UK; michel.michaelides@ucl.ac.uk.

Submitted: April 28, 2018
Accepted: July 13, 2018

Citation: Patterson EJ, Kalitzeos A, Kasilian M, et al. Residual cone structure in patients with X-linked cone opsin mutations. *Invest Ophthalmol Vis Sci*. 2018;59:4238–4248. https://doi.org/10.1167/iovs.18-24699

Purpose. To assess residual cone structure in subjects with mutations in exon 2, 3, and 4 of the *OPN1LW* or *OPN1MW* opsin.

Methods. Thirteen males had their *OPN1LW/OPN1MW* opsin genes characterized. The cone mosaic was imaged using both confocal and nonconfocal split-detection adaptive optics scanning light ophthalmoscopy (AOSLO), and retinal thickness was evaluated using optical coherence tomography (OCT). Six subjects completed serial imaging over a maximum period of 18 months and cone density was measured across imaging sessions.

Results. Ten subjects had an *OPN1LW/OPN1MW* "interchange" opsin mutation designated as LIAVA or LVAVA, which both introduce exon 3 splicing defects leading to a lack of functional photopigment in cones expressing LIAVA and greatly reduced functional photopigment in cones expressing LVAVA. Despite disrupted cone reflectivity and reduced numerosity, residual inner segments could be visualized. Similar patterns were observed in individuals with an exon 2 insertion, or an exon 4 splice defect, both of which are also expected to produce cones that are devoid of functional opsin protein. OCT revealed variably reduced retinal thickness. A significant inverse relationship was found between the proportion of waveguiding cones and axial length.

Conclusions. Split-detection imaging revealed that the altered appearance of the cone mosaic in confocal images for subjects with exon 2, 3, and 4 mutations was generally due to disrupted waveguiding, rather than structural loss, making them possible candidates for gene therapy to restore cone function. The relative fraction of waveguiding cones was highly variable across subjects, which appears to influence emmetropization in these subjects.

Keywords: myopia, color blindness, photoreceptor, retinal imaging

Bornholm eye disease (BED)[1,2] has been distinguished from other X-linked cone dysfunction syndromes by its association with red-green color vision deficiency, myopia, and astigmatism, in addition to other general cone dysfunction characteristics.[3] The disease in the original Danish family and in a Minnesota family with a similar phenotype was mapped to Xq28 (the locus of *MYP1*),[4] which encompasses the long (L) and middle (M) wavelength sensitive opsin genes *OPN1LW* and *OPN1MW,* respectively. Ultimately, the same underlying mutation in the cone opsin genes, designated LVAVA, was found in both families.[5,6] This "interchange-mutation" is associated with a combination of amino acids designated by the single letter code for the amino acids specified by exon 3 codons 153, 171, 174, 178, and 180, respectively, where L is leucine, V is valine, and A is alanine.[7] Although both of the original *MYP1* families had color vision deficiencies, which was a defining feature of BED, affected members of four additional families with X-linked high myopia of Chinese ancestry,[8–10] also mapped to *MYP1*, were later found to have normal color vision. The original (*MYP1*) families coincidentally had separate gene rearrangements responsible for their color vision deficiency, while the LVAVA mutation was responsible for the myopia and other cone dysfunction symptoms. In addition to altering the amino acid sequence, the underlying nucleotide combination introduces an exon 3 splicing defect that greatly reduces production of normal opsin. Cones expressing the mutant opsin appear to function well enough to support normal color vision in younger eyes but degenerate over time.[11] The malfunctioning cones lead to high myopia and cone degenerative symptoms in individuals with a submosaic of LVAVA-expressing cones, along with a submosaic of cones expressing normal pigment. The same mutation produces progressive cone dystrophy with significant vision loss by midlife in individuals who express LVAVA opsin in all L/M cones.[11]

Some individuals diagnosed as having BED, besides those in the original *MYP1* families, were found to have a different interchange mutation, designated LIAVA, which has isoleucine at position 171. This mutation was originally discovered as a cause of dichromacy in subjects who were not noted to have any of the pathological symptoms of BED.[12,13] Even though the

Table. Summary of the Genotype and Clinical Phenotype of Subjects With X-Linked Cone Dysfunction

	Subject	Age, y	Phenotype	Genotype	Mutation Type	Axial Length, mm		Source
						OD	OS	
1	JC_0084	37	Deuteranope	L - M_{LIAVA}	interchange: exon 3	25.34	25.19	Subject NC[12]
2	MM_0133	29	Protanope	L_{LIAVA} - M - M	interchange: exon 3	27.48	27.32	Subject B1[32] / JC_0195[6]
3	MM_0142	15	Protanope	L_{LIAVA} - M	interchange: exon 3	23.34	23.28	MM_0142[6]
4	MM_0144*	19	Protanope	M_{LIAVA} - M	interchange: exon 3	27.14	26.90	Subject C1[6,32]
5	MM_0145*	16	Protanope	M_{LIAVA} - M†	interchange: exon 3	23.57	23.59	Subject C2[6,32]
6	MM_0155‡§	30	Unclassified RG defect	L_{LIAVA} - M	interchange: exon 3	30.74	29.51	This study
7	JC_0609	15	Protanope	L_{LIAVA} - M	interchange: exon 3	29.03	29.08	JC_0609[6]
8	JC_10340§	32	Protanope	M_{LVAVA} - M - M	interchange: exon 3	28.96	28.08	Subject 31[4] / JC_10340[6]
9	JC_11437*	36	Deuteranope	L_{LVAVA} - L - M - M	interchange: exon 3	25.04	23.92	Subject 96[1]
10	JC_11445*	26	Deuteranope	L_{LVAVA} - L - M - M	interchange: exon 3	25.79	25.65	This Study
11	MM_0156*	13	Protanope	$L_{exon\ 2\ insertion}$ - M	insertion: exon 2	27.90	28.24	MM_0156[6]
12	MM_0157*	18	Protanope	$L_{exon\ 2\ insertion}$ - M	insertion: exon 2	23.69	23.57	MM_0157[6]
13	MM_0188	10	Unclassified RG defect	$L_{exon\ 4\ splice\ defect}$ - M	splice defect: exon 4	24.99	24.89	This study

* The following subjects are brothers: MM_0144 and MM_0145; JC_11437 and JC_11445; MM_0156 and MM_0157.
† MM_0145 was not genetically sequenced; genotype was inferred from brother (MM_0144) based on their mother's normal color vision.
‡ OCT images from MM_0155 were not analyzable.
§ AOSLO images from MM_0155 and JC_10340 were not analyzable.

LVAVA and the LIAVA genes and their encoded proteins are similar, they produce striking differences in phenotype.[14] Most notable are (1) that no function from LIAVA cones can be detected in psychophysical or ERG measurements, so people expressing LIAVA are obligate dichromats (or blue cone monochromats if all the *OPN1LW/OPN1MW* genes express it), and (2) disorders associated with LIAVA appear to be spared from some of the detrimental effects associated with LVAVA that result from the expression of small amounts of correctly spliced LVAVA protein, which is apparently toxic to the cell.[14,15]

Confocal adaptive-optics scanning light ophthalmoscopy (AOSLO) has been used to demonstrate variable reduction in the density of normally waveguiding cones among subjects with various *OPN1LW/OPN1MW* mutations.[6,11,12,16] One drawback of confocal AOSLO imaging is its reliance on the ability of cone photoreceptors to effectively waveguide light, making it difficult to ascertain whether dark areas are indicative of cone loss or simply altered waveguiding. For example, although numerous dark spaces are evident in confocal retinal images from subjects with achromatopsia,[12,17] nonconfocal split-detection imaging has revealed residual cone structure within these areas.[17,18] Split-detection imaging exploits light that is multiply-scattered by the retina, which enables visualization of the cone inner segments in a manner thought to be independent of their waveguiding properties[17,19]; the simultaneous acquisition of both modalities provides direct temporal correspondence and coaxial alignment ensures direct spatial correspondence between bright spots or dark gaps in confocal images and cone structure in split-detection images. Here we used AOSLO to characterize cone structure in subjects harboring the LIAVA or LVAVA exon 3 haplotype, and compared these findings with subjects with mutations in exon 2 and 4. We also examined longitudinal changes in retinal structure using optical coherence tomography (OCT) and AOSLO. Given the growing emergence of therapeutic trials for cone disorders, there is an increased need to stratify patients for potential participation and to establish outcome measures to assess treatment efficacy[20,21]; the successful use of AOSLO to examine challenging conditions such as X-linked cone dysfunction demonstrates its potential utility in such trials.

Materials and Methods

Subjects

Thirteen male subjects with red-green color vision deficiency and/or suspected X-linked cone dysfunction were recruited. The genotype and clinical phenotype for nine of the subjects has been reported previously (Table). The four remaining subjects provided blood samples, from which DNA was isolated and opsin genes were amplified and sequenced using previously described methods.[13,22] Axial length was measured in each eye imaged using the Zeiss IOL Master (Carl Zeiss Meditec, Dublin, CA, USA). Color vision was assessed using the Richmond HRR (4th edition), the Rayleigh match and the Colour Assessment and Diagnosis[23] test when available. This study followed the tenets of the Declaration of Helsinki and was approved by local institutional review boards (MCW: PRO17439 & PRO30741). Informed consent was obtained from all subjects, after the nature and possible consequences of the study were explained.

Spectral-Domain Optical Coherence Tomography (SD-OCT)

High-resolution SD-OCT images of the macula were acquired using the Bioptigen Envisu R2200 SD-OCT system (Leica Microsystems, Wetzlar, Germany). High-density line scans (either 750 or 1000 A-scans/B-scan, 100–150 repeated B scans) were acquired through the foveal center. Line scans were registered and averaged to reduce speckle noise in the image and then scaled as previously described.[6] Longitudinal reflectance profiles were created from logarithmic grayscale images using custom software—OCT Reflectivity Analytics[24]—to yield measurements of total retinal thickness as well as outer nuclear layer and Henle fiber layer (ONL+) thickness at the fovea.

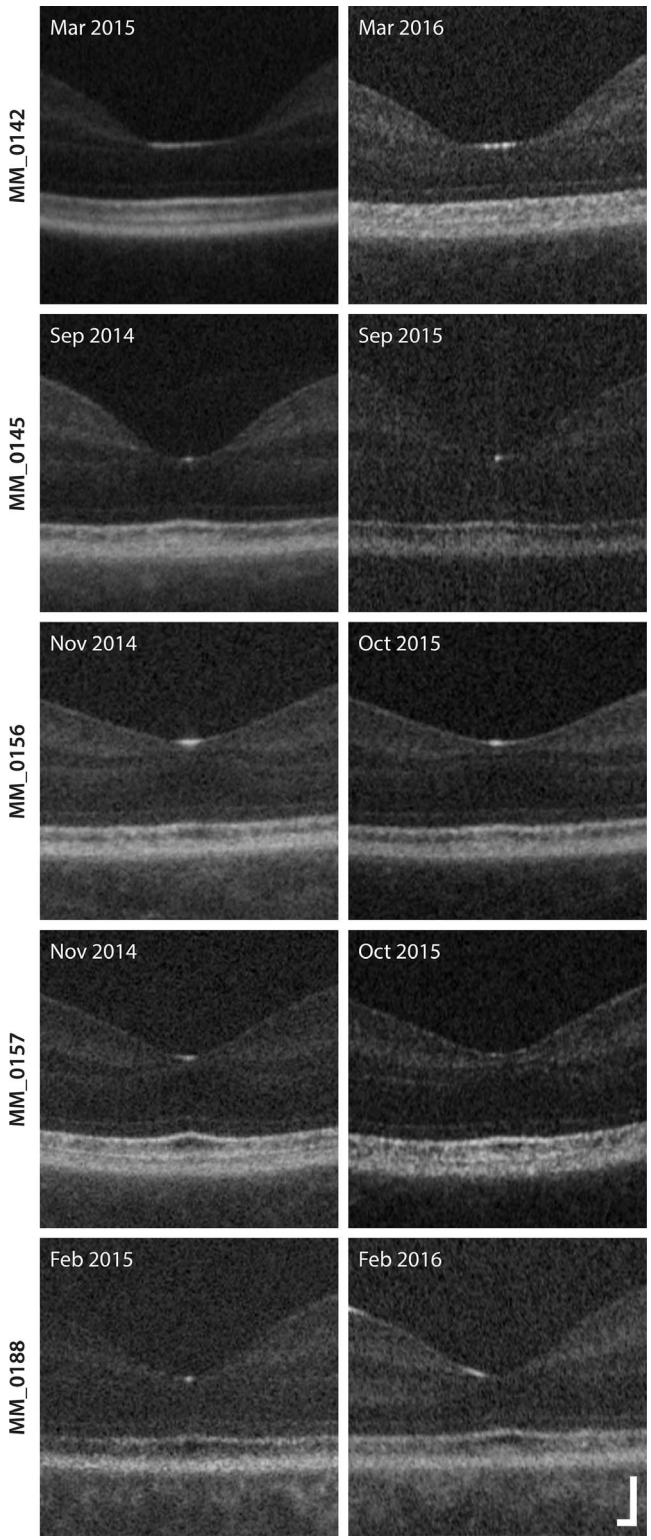

Figure 1. Longitudinal OCT showed no evidence of retinal thinning at the fovea over a follow-up period of 12 months in five subjects. Two with LIAVA, two with an exon 2 insertion, and one with an exon 4 splice defect. Foveal scans are shown for each of the five subjects analyzed on initial examination (*left*) and after 1 year (*right*). *Scale bar*: 100 μm.

Adaptive Optics Retinal Imaging

Each eye imaged was dilated using one drop of phenylephrine hydrochloride (2.5%) and one drop of tropicamide (1%). Confocal and split-detection videos of the central photoreceptor mosaic were obtained with one of two previously described AOSLO systems, housed either at the Medical College of Wisconsin or at Moorfields Eye Hospital.[6,17] Raw videos were registered and averaged to produce images with a high signal-to-noise ratio, which were then montaged as previously described.[6,25]

For 10 subjects, the foveal center was identified using the 'peak cone density' method, as previously described.[6,26] Where possible, this was achieved using confocal images; however, the severely reduced reflectivity of foveal cones for JC_0609 made this unfeasible, so split-detection was used. Due to poor image quality and inability to resolve foveal cones for MM_0156, the 'preferred retinal locus' method was used, as previously described.[6] For the remaining two subjects, image quality was too poor to enable further analysis.

A semiautomated algorithm was used to mark the location of individual cones in each 55-μm region of interest (ROI),[27] and the coordinates were used to calculate cone density, when possible, at the fovea, as well as at 0.25°, 0.5°, and at 1° intervals from 1° to 10° along the temporal meridian. Each ROI was counted twice by a single observer (EJP) to assess repeatability and the mean was used for subsequent analysis.

Follow-up data were available for six subjects, enabling us to monitor cone density across two or more time points. The largest available montage was chosen as the "reference" montage, to which all other montages were scaled and aligned. ROIs were located manually, ensuring that the same locations were assessed across imaging sessions. To correct for differences in distortion between montages, follow-up images were warped to the reference image using Fiji's plugin, bUnwarpJ.[28] Due to changes in the size of montages acquired across imaging sessions and sites, only ROIs at the fovea and at 0.25°, 0.5°, and 1° were used in longitudinal assessment. Cone density was measured using both confocal and split-detection modalities wherever possible. GraphPad Prism (La Jolla, CA, USA) was used for statistical analysis.

Results

A summary of the genotype and clinical phenotype for each patient is given in the Table. Ten subjects were found to have exon 3 haplotypes, seven with LIAVA and three with LVAVA. In LIAVA, exon 3 is skipped and exon 2 is spliced directly to exon 4, the splicing defect has been shown to be "complete," leading to a total lack of functional photopigment and a stationary phenotype.[15,29,30] In LVAVA, the splicing defect has been shown to be "incomplete," resulting in a small amount of full-length mRNA and a small amount of functional photopigment; although this has been associated with residual function, protein toxicity can lead to progressive cone degeneration.[14,15] Two subjects had exon 2 insertions, which can result in alterations in secondary RNA structure, protein coding sequences or splicing.[31] The remaining subject had an exon 4 splice defect (IVS4+1G>T).

Among subjects with LIAVA (n = 7), axial length was generally greater than for normal emmetropia (24.00 ± 1.09 mm),[33] with a mean ± SD of 26.5 ± 2.6 mm, although three of these subjects (MM_0142, MM_0145, and MM_0157) were within the normal range.

Retinal thickness was measured at the fovea for 12 subjects. Total retinal thickness (180.51 ± 18.74 μm) at the fovea ranged from 69% to 97% of normal, while ONL+ thickness (79.64 ±

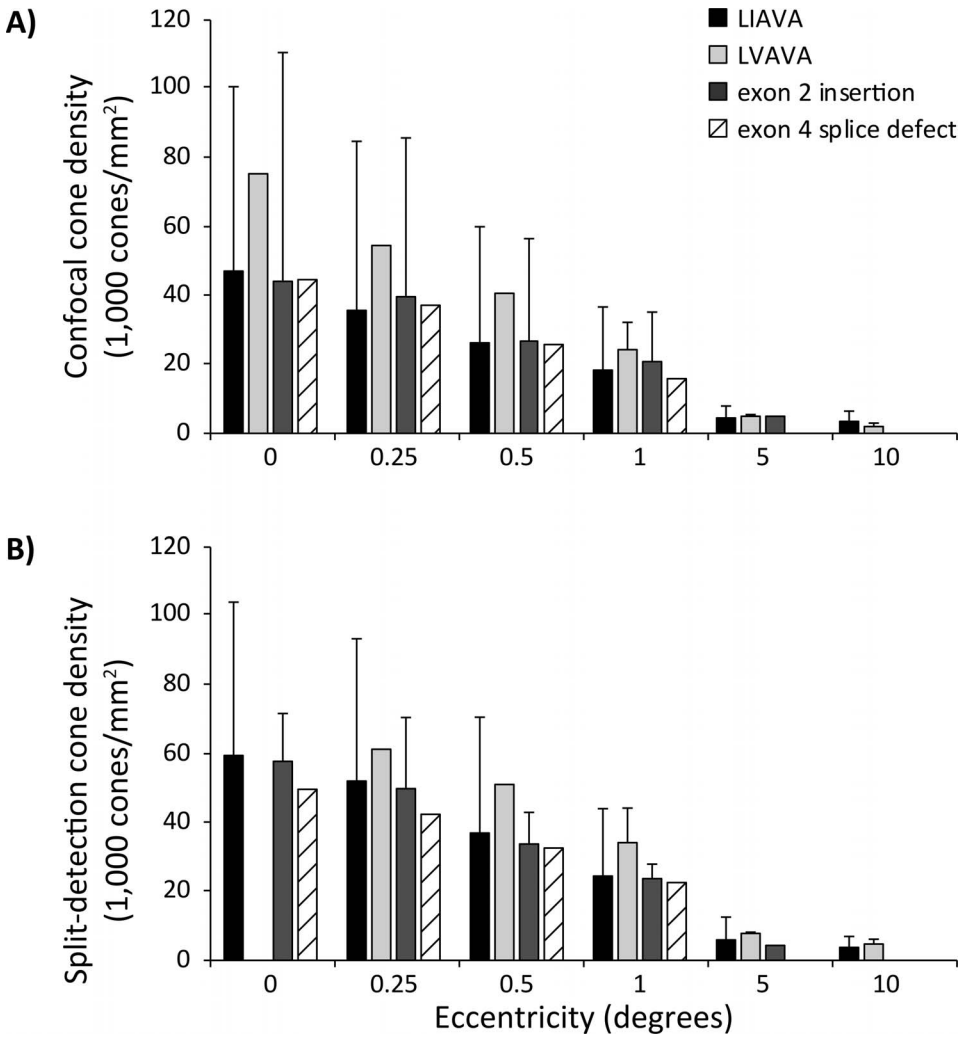

FIGURE 2. Confocal (**A**) and split-detection (**B**) cone density values are shown grouped by type of mutation. Where there are data from more than one subject, means and 2 SDs are shown. Cones were present in all ROIs for all analyzable subjects, therefore, the absence of *bars* or *error bars* indicates that there was insufficient data. Density measured using split-detection was consistently higher than confocal images, indicating the presence of nonwaveguiding cones.

14.12 μm) ranged from 51% to 96% of normal.[6] Additionally, we analyzed retinal thickness over a 12-month period for five subjects using OCT (Fig. 1). We found no evidence for change in either total retinal thickness ($P = 0.405$) or ONL+ thickness ($P = 0.392$) at the fovea over the course of 12 months.

Cone density was examined in 11 of 13 subjects, while the images obtained from the remaining two subjects were of insufficient quality to enable accurate quantification; these subjects were excluded from further analysis. Mean cone density values from a single time point are shown grouped by the type of mutation in Figure 2 (for all mean density values for each subject at all available locations, see Supplementary Table S1).

Due to changes in cone topography across the retina, the density data did not have a normal distribution. After log transformation, confocal data remained nonnormal ($P < 0.01$) whereas the split-detection data passed the normality test ($P = 0.069$). Given the borderline P value, we opted to use nonparametric methods to compute the limits of agreement in the Bland-Altman plots, shown in Figure 3. In the case of confocal images, the discrepancy was larger when cone density was low, whereas for split-detection, the discrepancy was relatively constant. These effects are likely owing to increased ambiguity at more eccentric locations; larger multimodal cones, the presence of rods, and increased nystagmus are all factors that impact the reliability of cone identification in peripheral confocal images. The presence of a relationship between density and the size of discrepancy using confocal images suggests that cone identification using split-detection images may be less susceptible to location-dependent changes in accuracy. The intraclass correlation coefficient for the two sets of split-detection (log) counts across all available locations was 0.98 (subject SD = 1.01, residual SD = 0.14).

In agreement with previous findings,[6] our subjects showed variably reduced foveal density from normal (~85,000–235,000 cones/mm^2),[26,34] with a mean ± SD of 49,155 ± 24,459 cones/mm^2 (range, 19,061–90,970 cones/mm^2) using confocal images. Likewise, split-detection cone density (57,845 ± 18,010 cones/mm^2; range, 29,750–96,625 cones/mm^2) fell below the normal range for all but one subject (JC_0084, for whom the LIAVA mutation was expressed by the second gene in the array). However, density measured using split-detection images was significantly greater than confocal ($P < .0001$, Wilcoxon matched pairs t-test). A direct correspondence

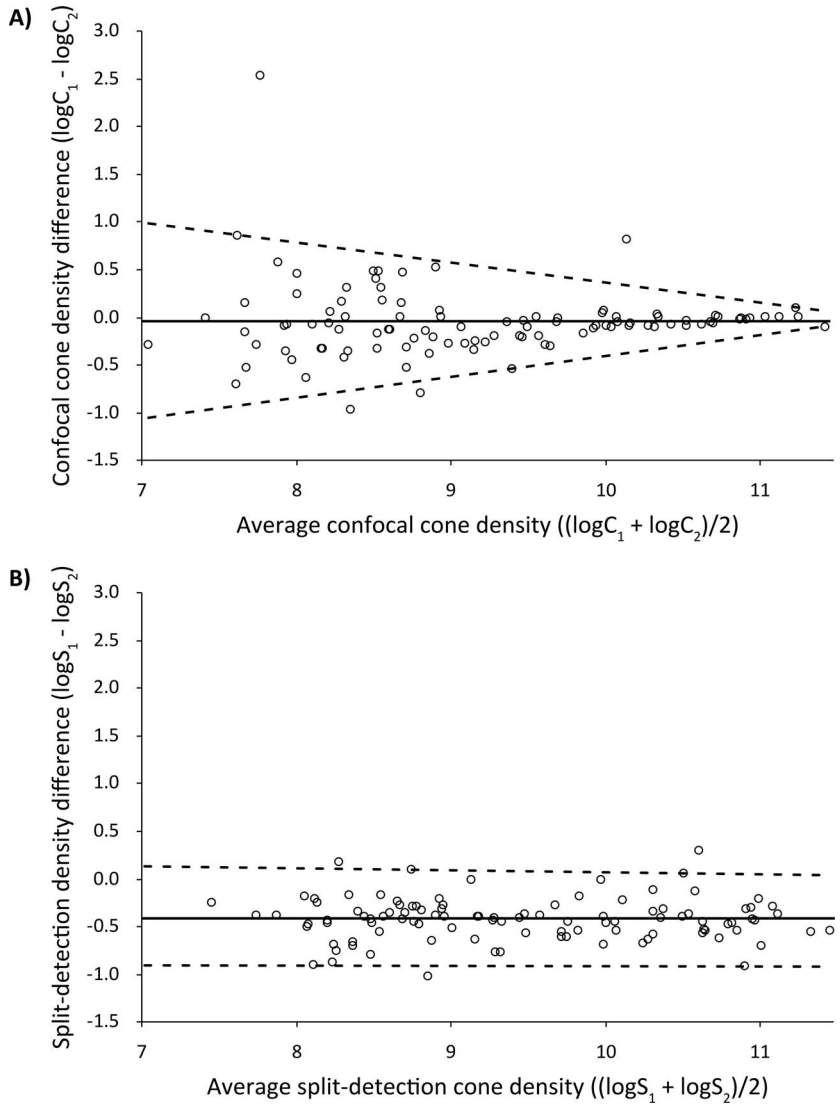

Figure 3. Bland-Altman plot, showing the distribution of differences for repeated cone counts by the same observer. All retinal locations are included in analysis, resulting in nonnormal distribution and subsequent log transformation. Bias (*solid line*) and nonparametric limits of agreement (*dotted lines*) for both confocal (**A**) and split-detection (**B**) are shown. Cone identification shows a location-based bias in reliability, whereas split-detection images show similar differences across the retina.

between dark gaps observed in confocal images and inner segment structure in split-detection images can be seen in four LIAVA subjects (Fig. 4) and one subject from each of the remaining mutation types in (Fig. 5).

There was a statistically significant inverse relationship between axial length and the proportion of foveal cones that effectively waveguide light (calculated as confocal/split-detection counts × 100; $P = 0.043$, Spearman $r = 0.70$; Fig. 6), using AOSLO data from nine subjects, indicating a correlation between eye growth and the proportion of functioning cones in the mosaic. Direct observation of the images for LIAVA subjects in Figure 4 would also suggest that those with the highest axial lengths have the fewest waveguiding cones. Although retinal magnification and retinal stretching in myopia has the potential to affect the conversion between angular and retinal distance units, as well as the "true" number of cones,[35] the proportion of cones that are visibly waveguiding is not confounded by these factors.

No relationship was found between total retinal thickness and foveal cone density as measured using either confocal ($P = 0.588$) or split-detection images ($P = 0.387$). There was also no relationship between ONL+ thickness and either confocal ($P = 0.770$) or split-detection ($P = 0.710$) foveal cone density.

We were able to obtain images at two or more time points (6, 12, and/or 18 months) for six of 11 analyzable subjects (MM_0142, MM_0144, MM_0145, MM_0156, MM_0157, MM_0188). As there were more time points for which cone density was quantifiable at 0.5° temporal, rather than at foveal center, we used this location for longitudinal analysis (Fig. 7). There were large fluctuations in cone density, with a mean ± SD density increase of 2 ± 12% for confocal and 21 ± 33% for split-detection images. Linear modeling revealed no significant slope for either confocal ($P = 0.692$) or split-detection ($P = 0.485$) modalities. For some subjects (JC_0084, JC_0609, MM_0142, MM_0145, MM_0188), confocal imaging revealed localized areas of reduced reflectivity that were not necessarily present at all visits (Fig. 8).

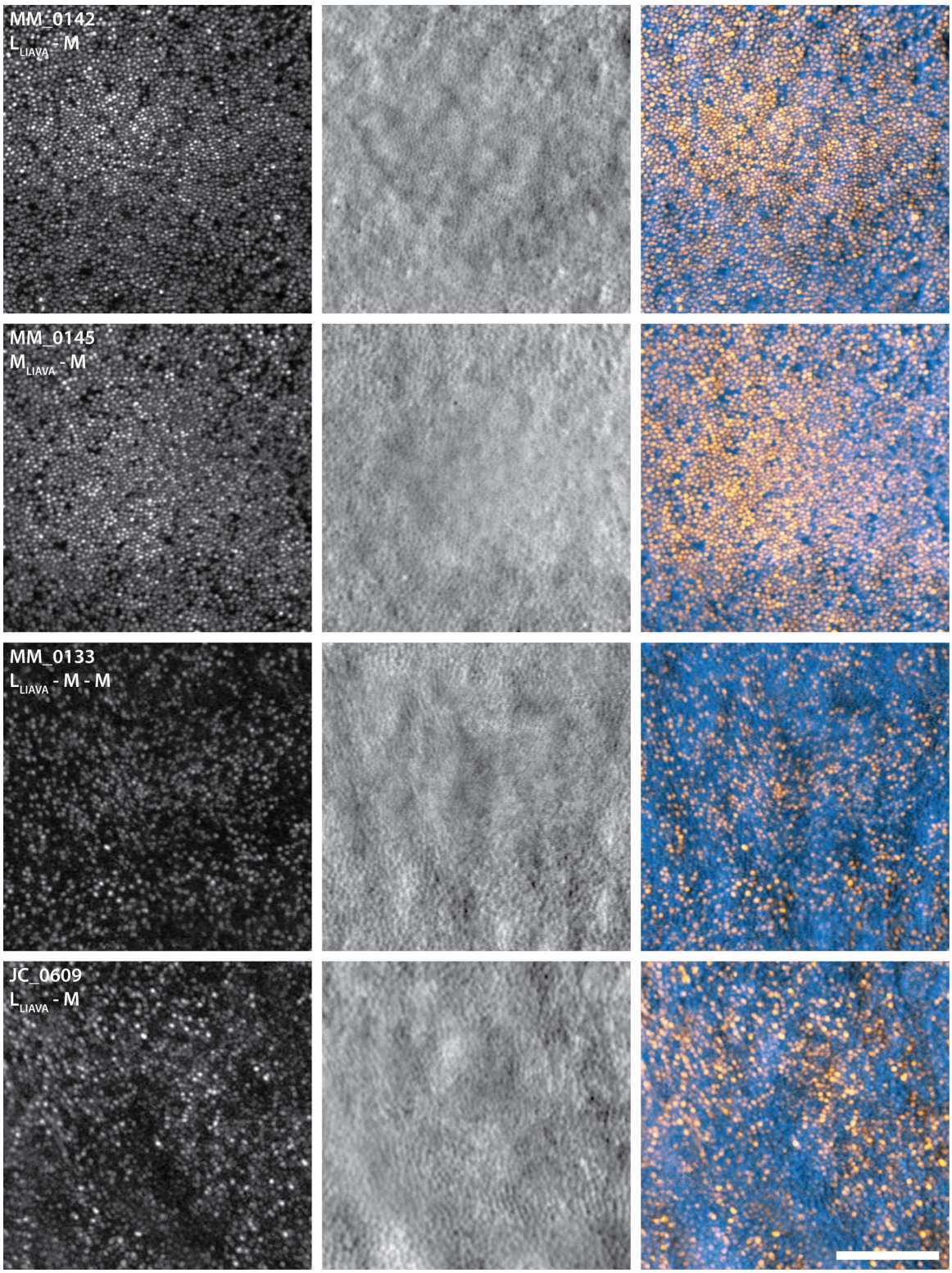

Figure 4. Confocal (column 1) and split-detection (column 2) AOSLO images of the foveal center for four subjects with the LIAVA haplotype. Also shown are color-merged images (column 3) in which *amber* represents the brightly reflective cones and rods visible in the confocal channel and *blue* represents the structure shown in split-detection images. The subjects in the *upper two rows* have the shortest axial length (23.34 and 23.59 mm) and the subjects in the *lower two rows* have the longest (27.48 and 29.03 mm) of the analyzable LIAVA subcohort. The proportion of area occupied by visibly waveguiding cones is higher for the subjects with shorter axial length than those with longer axial length, illustrating the significant relationship found between axial length and waveguiding to nonwaveguiding cone ratio. *Scale bar*: 100 μm.

Investigative Ophthalmology & Visual Science

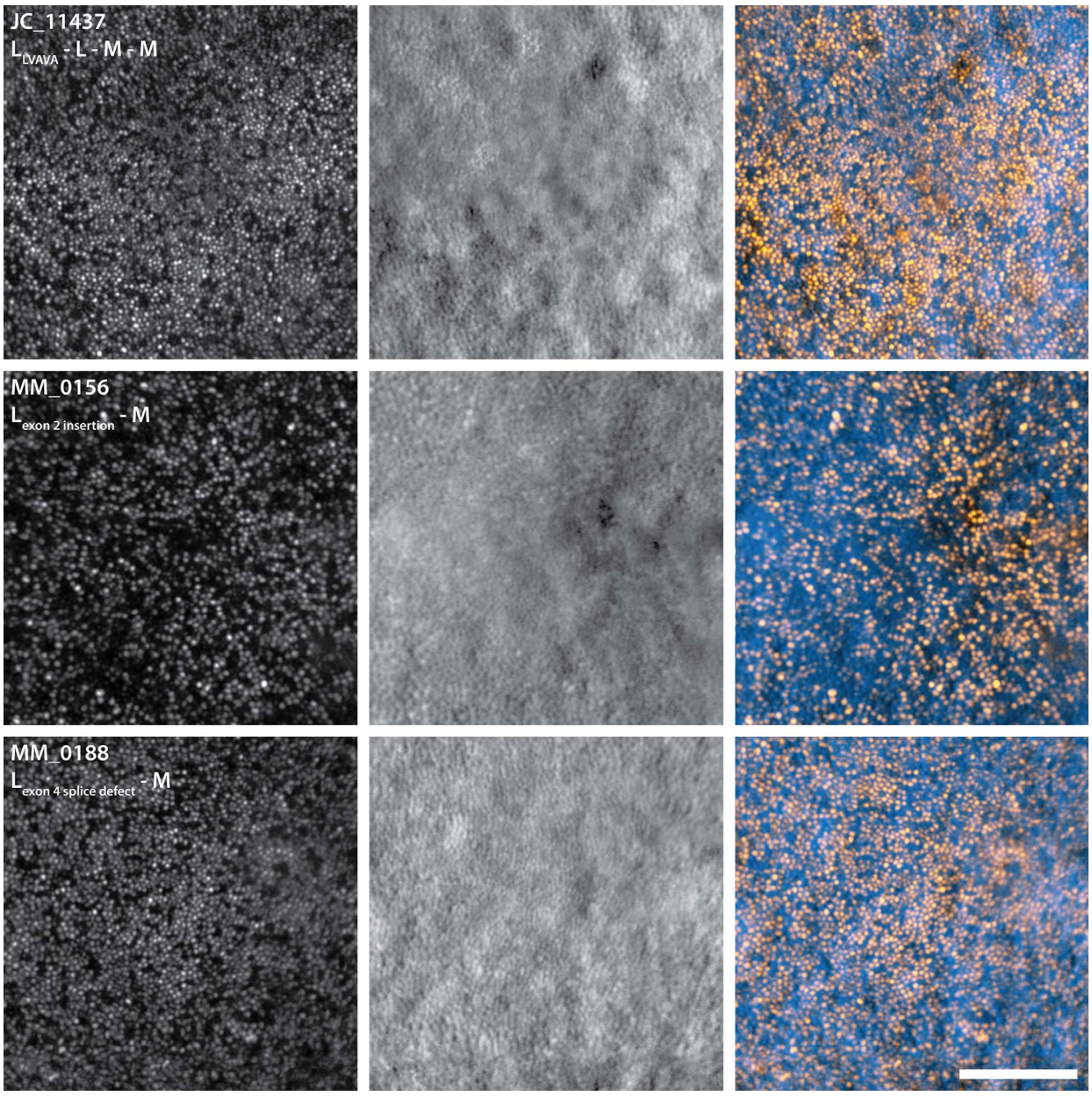

FIGURE 5. Confocal (column 1) and split-detection (column 2) AOSLO images of the foveal center for subjects with the exon 3 LVAVA haplotype, exon 2 insertion, and exon 4 splice defect. Also shown are color-merged images (column 3) in which *amber* represents the brightly reflective cones and rods visible in the confocal channel and *blue* represents the structures shown in split-detection images. Although the ratio of waveguiding to nonwaveguiding cones is variable, similar overall appearance is observed across mutations. *Scale bar*: 100 μm.

DISCUSSION

The current study used high-resolution split-detection AOSLO imaging to characterize the structural integrity of the retinal mosaic in subjects with X-linked cone dysfunction. We present the first definitive evidence of residual cone inner segments, albeit with reduced density from normal, in those harboring *OPN1LW/OPN1MW* mutations. This highlights the utility of split-detection images (in which cones were identifiable despite the absence of waveguiding) and contributes to the growing body of work that has revealed inner segment structure in various pathologies known to reduce or abolish cone function.[18,36]

While, on average, we found no evidence of progressive cone loss in subjects with LIAVA, exon 2 insertion, or exon 4 splice defect mutations, a limitation of this study was the moderate fluctuation in measured cone density across time points. Both modalities likely incurred errors in cone identification as has been previously reported,[27,37] with split-detection showing higher variability than confocal values. However, measurement error has been shown to be disease-specific,[36] and the split-detection data we present here are the first of their kind for X-linked cone dysfunction. As this subject population had relatively high foveal cone density when compared with conditions like achromatopsia,[18] the size of parafoveal cones approached the resolution limit of split-

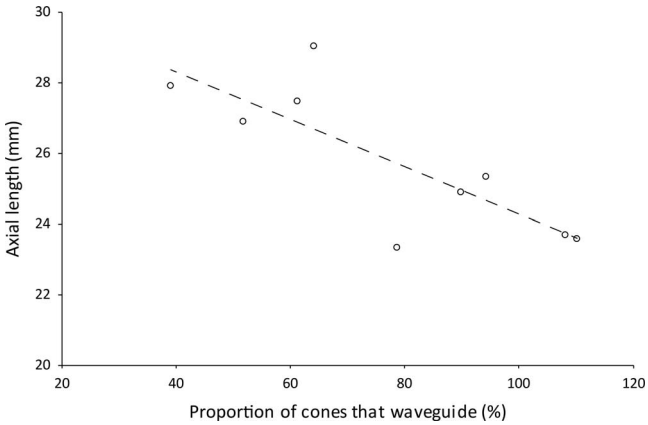

FIGURE 6. The assumed proportion of foveal cones that effectively waveguide light (calculated as confocal / split-detection counts × 100) decreases with increasing axial length ($P = 0.043$, Spearman $r = 0.70$). This inverse relationship lends support to the theory that the number of nonfunctional cones within the retina plays a significant role in myopia progression.

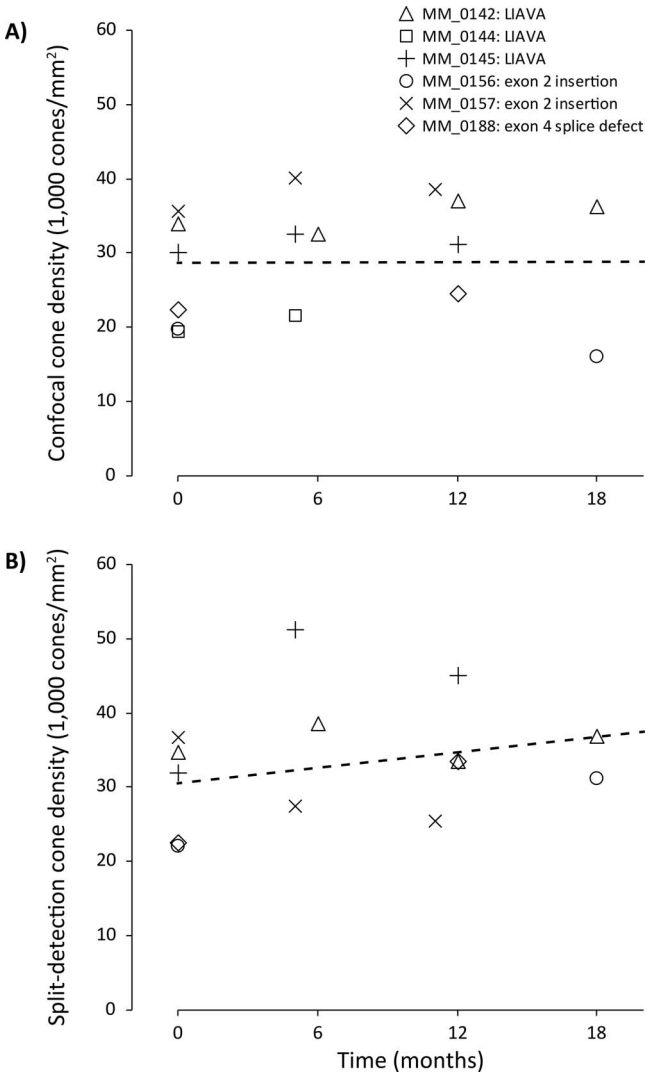

FIGURE 7. Parafoveal cone density at 0.5° temporal, assessed using both confocal (**A**) and split-detection (**B**) modalities, showed no significant change over an 18-month follow-up period for six subjects. Three with LIAVA, two with an exon 2 insertion and one with an exon 4 splice defect. A linear model revealed no significant slope for either confocal ($P = 0.692$) or split-detection ($P = 0.485$) density.

detection AOSLO, thereby increasing susceptibility to misidentification. Although not significant, the overall trend for the split-detection data was toward an increase in cone density, as has been noted in other longitudinal studies.[38] Image quality can influence the accuracy of cone identification; nystagmus, fixational stability, and subject cooperation all tend to improve with a subject's age and experience. This might suggest the need to develop more extensive baseline testing similar to those designed to account for learning effects in visual field testing. For confocal AOSLO, changes in cone reflectivity over time (Fig. 8) may be a source of error, though we tried to avoid using ROIs containing large areas of low reflectivity. Even within a single image, the high variability in cone reflectivity in these subjects introduces uncertainty in differentiating between nonreflecting and dimly reflecting cones, which impacts the accuracy of cone identification using confocal AOSLO images. This is supported by recent work showing that observers require less training to converge on agreement when identifying cones using split-detection AOSLO compared with confocal AOSLO.[39] There is also evidence that observer training and experience can significantly affect repeatability in cone identification.[36,39,40] As such, automated cone detection techniques that use both confocal and split-detection modalities may facilitate more objective and reliable quantification.[41]

The LIAVA haplotype produces an exon 3 splicing defect, this causes exon 2 to be spliced to exon 4 causing a reading frameshift, resulting in a stop codon that subjects the mRNA to nonsense mediated decay,[30,42,43] thus accounting for the complete absence of any measurable function of LIAVA-expressing cones. Previous work indicates that the LVAVA interchange mutation results in misfolded or dysfunctional opsin and is associated with late onset cone degeneration.[11,14] However, in stark contrast to previous reports of severe localized degeneration of foveal photoreceptors in LVAVA patients,[6,11] split-detection images of the two brothers studied here (JC_11437 and JC_11445) showed a contiguous foveal cone mosaic. It is unclear whether this finding indicates a particularly late onset of cone degeneration, as they are aged 36 and 26 years, respectively, or whether these brothers are genuine examples of a more stationary LVAVA phenotype. Comprehensive genetic analysis and longitudinal imaging using a larger LVAVA cohort is necessary to determine the degree of progression attributable this opsin variant.

This study lends insight into mechanisms underlying myopia. The first reported AOSLO images from a person with LIAVA was a deuteranope with the mutation in the second gene of the array (JC_0084).[12] While the individual did have a mild refractive error, other symptoms associated with X-linked cone dysfunction (beyond the color defect) would be expected to be minimal as, for the average Caucasian, more than two-thirds of the cones express the first gene in the array.[44] Six of seven LIAVA patients reported here had the mutation in the first gene in the array, and four of those had extremely high-grade myopia with refractive errors predicted to average greater than 10 diopters; those who were analyzable also had fewer waveguiding cones. Similarly, of the two brothers with an exon 2 insertion, MM_0156 had the largest disparity in density between modalities and also had a longer axial length. Differences such as this between brothers with the same

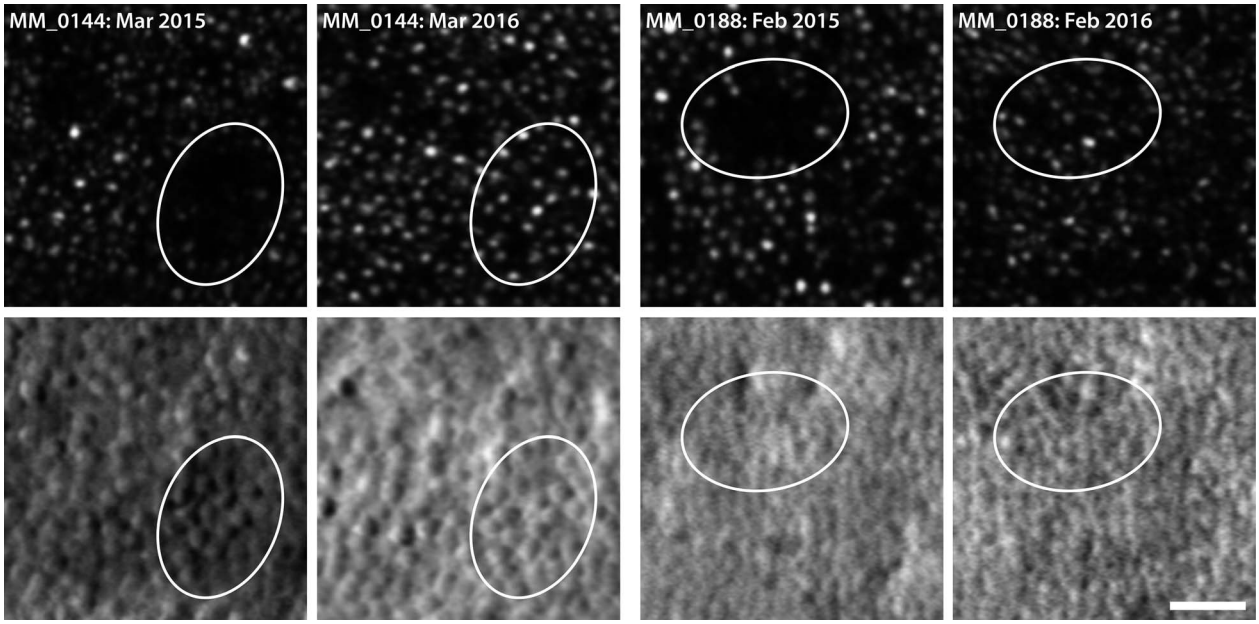

Figure 8. Confocal AOSLO (*upper row*) reveals distinct patches of reduced cone reflectivity, which, by itself, might indicate changes over time. However, split-detection imaging (*lower row*) enables visualization of intact cone inner segments within these areas of low reflectivity. Furthermore, split-detection images, unlike confocal, show perfect registration across timepoints, highlighting the utility of this imaging modality, particularly in longitudinal assessment. Images are from MM_0142 (LIAVA) and MM_0188 (exon 4 splice defect) at approximately 1° from the foveal center. *Scale bar*: 25 μm.

genotype may be explained by differences in the relative expression of first versus downstream genes in the array, which is what typically produces individual differences in L/M cone ratio among trichromatic individuals (even brothers).[6] In subjects MM_0142 and MM_0145, skewed/reduced expression of the first gene (LIAVA) in their arrays (which would lead to a low L/M cone ratio in normal individuals) likely results in relatively few nonwaveguiding cones, hence their minimal myopia. As the relative expression of first versus downstream genes in the array is determined early in development,[45] our results suggest a causative relationship between the relative fraction of nonfunctional/nonwaveguiding cones and myopia severity. Previously, the relationship between myopia and the activity of ON-bipolar cells has been noted.[14] As shown here, patients with an LIAVA opsin gene clearly have cone inner segments where sodium is pumped out, but they lack photopigment and visible outer segments where the cation channels required for depolarization are normally located. Thus, they are expected to be constitutively hyperpolarized, preventing the release of glutamate required to inhibit ON-bipolar cells. This would explain the correlation between the number of LIAVA-expressing cones and myopia; the greater the number of defective cones that cannot release glutamate normally in the dark, the greater the disinhibition of ON-bipolar signaling, which is responsible for signaling the eye to grow.

The LIAVA haplotype has been previously associated with a stationary phenotype.[12–14] Similarly, the splice defect and insertion studied here also introduce stop codons that would signal nonsense–mediated decay of the mRNA, and thereby predict a stationary phenotype, although, owing to the small sample size, this finding has low statistical power. Future longitudinal analysis should aim to include greater numbers of subjects with each underlying mutation, as well as longer duration of follow-up, to determine the therapeutic window for these patients. Regardless, it appears from the results presented here that cones devoid of opsin remain viable, suggesting that many of these subjects may be appropriate candidates for gene therapy efforts to restore cone function.

Acknowledgments

The authors thank Robert F. Cooper, Brian P. Higgins, Christopher S. Langlo, Alex E. Salmon, Phyllis Summerfelt, and Melissa Wilk for their contributions to this work. They also thank Sergey Tarima and Alexis Visotcky for statistical support.

Supported by grants from the National Center for Research Resources and the National Center for Advancing Translational Sciences of the National Institutes of Health under award number UL1TR001436 (Bethesda, MD, USA) and by the National Eye Institute of the National Institutes of Health under award numbers R01EY017607, R01EY021242, R01EY028118, P30EY001931, P30EY001730 (Bethesda, MD, USA). This investigation was conducted in part in a facility constructed with support from the Research Facilities Improvement Program, grant number C06RR016511 from the National Center for Research Resources, National Institutes of Health (Bethesda, MD, USA). Additional support came from an unrestricted grant from Research to Prevent Blindness (New York, NY, USA), Foundation Fighting Blindness (Columbia, MD, USA), Moorfields Special Trustees (London, UK), Moorfields Eye Charity (London, UK), Fight for Sight (London, UK), Medical Research Council (London, UK), and the National Institute for Health Research Biomedical Research Centre at Moorfields Eye Hospital NHS Foundation Trust and UCL Institute of Ophthalmology (London, UK). MM is the recipient of a Career Development Award from the Foundation Fighting Blindness.

Disclosure: **E.J. Patterson**, None; **A. Kalitzeos**, None; **M. Kasilian**, None; **J.C. Gardner**, None; **J. Neitz**, None; **A.J. Hardcastle**, None; **M. Neitz**, None; **J. Carroll**, None; **M. Michaelides**, None

References

1. Haim M, Fledelius HC, Skarsholm D. X-linked myopia in a Danish family. *Acta Ophthalmol*. 1988;66:450–456.

2. Schwartz M, Haim M, Skarsholm D. X-linked myopia: Bornholm eye disease. Linkage to DNA markers on the distal part of Xq. *Clin Genet*. 1990;38:281–286.
3. Aboshiha J, Dubis AM, Carroll J, Hardcastle AJ, Michaelides M. The cone dysfunction syndromes. *Br J Ophthalmol*. 2016; 100:115–121.
4. Young TL, Deeb SS, Ronan SM, et al. X-linked high myopia associated with cone dysfunction. *Arch Ophthalmol*. 2004; 122:897–908.
5. McClements M, Davies WI, Michaelides M, et al. Variations in opsin coding sequences cause X-linked cone dysfunction syndrome with myopia and dichromacy. *Invest Ophthalmol Vis Sci*. 2013;54:1361–1369.
6. Patterson EJ, Wilk M, Langlo CS, et al. Cone photoreceptor structure in patients with X-linked cone dysfunction and red-green color vision deficiency. *Invest Ophthalmol Vis Sci*. 2016;57:3853–3963.
7. Neitz J, Neitz M. The genetics of normal and defective color vision. *Vision Res*. 2011;51:633–651.
8. Guo X, Xiao X, Li S, Wang P, Jia X, Zhang Q. Nonsyndromic high myopia in a Chinese family mapped to MYP1: linkage confirmation and phenotypic characterization. *Arch Ophthalmol*. 2010;128:1473–1479.
9. Li J, Gao B, Guan L, et al. Unique variants in OPN1LW cause both syndromic and nonsyndromic X-linked high myopia mapped to MYP1. *Invest Ophthalmol Vis Sci*. 2015;56:4150–4155.
10. Ratnamala U, Lyle R, Rawal R, et al. Refinement of the X-linked nonsyndromic high-grade myopia locus MYP1 on Xq28 and exclusion of 13 known positional candidate genes by direct sequencing. *Invest Ophthalmol Vis Sci*. 2011;52:6814–6819.
11. Carroll J, Dubra A, Gardner JC, et al. The effect of cone opsin mutations on retinal structure and the integrity of the photoreceptor mosaic. *Invest Ophthalmol Vis Sci*. 2012;53: 8006–8015.
12. Carroll J, Neitz M, Hofer H, Neitz J, Williams DR. Functional photoreceptor loss revealed with adaptive optics: an alternate cause of color blindness. *Proc Natl Acad Sci U S A*. 2004;101: 8461–8466.
13. Neitz M, Carroll J, Renner A, Knau H, Werner JS, Neitz J. Variety of genotypes in males diagnosed as dichromatic on a conventional clinical anomaloscope. *Vis Neurosci*. 2004;21: 205–216.
14. Greenwald SH, Kuchenbecker JA, Rowlan JS, Neitz J, Neitz M. Role of a dual splicing and amino acid code in myopia, cone dysfunction and cone dystrophy associated with L/M opsin interchange mutations. *Trans Vis Sci Tech*. 2017;6(3):2.
15. Gardner JC, Liew G, Quan YH, et al. Three different cone opsin gene array mutational mechanisms with genotype-phenotype correlation and functional investigation of cone opsin variants. *Hum Mutat*. 2014;35:1354–1362.
16. Cideciyan AV, Hufnagel RB, Carroll J, et al. Human cone visual pigment deletions spare sufficient photoreceptors to warrant gene therapy. *Hum Gene Ther*. 2013;24:993–1006.
17. Scoles D, Sulai YN, Langlo CS, et al. In vivo imaging of human cone photoreceptor inner segments. *Invest Ophthalmol Vis Sci*. 2014;55:4244–4251.
18. Langlo CS, Patterson EJ, Higgins BP, et al. Residual foveal cone structure in CNGB3-associated achromatopsia. *Invest Ophthalmol Vis Sci*. 2016;57:3984–3995.
19. Scoles D, Flatter JA, Cooper RF, et al. Assessing photoreceptor structure associated with ellipsoid zone disruptions visualized with optical coherence tomography. *Retina*. 2016;36:91–103.
20. Luo X, Cideciyan AV, Iannaccone A, et al. Blue cone monochromacy: visual function and efficacy outcome measures for clinical trials. *PLoS One*. 2015;10:e0125700.
21. Cideciyan AV, Roman AJ, Jacobson SG, et al. Developing an outcome measure with high luminance for optogenetics treatment of severe retinal degenerations and for gene therapy of cone diseases. *Invest Ophthalmol Vis Sci*. 2016; 57:3211–3221.
22. Carroll J, Baraas RC, Wagner-Schuman M, et al. Cone photoreceptor mosaic disruption associated with Cys203Arg mutation in the M-cone opsin. *Proc Natl Acad Sci U S A*. 2009;106:20948–20953.
23. Rodriguez-Carmona ML, Harlow AJ, Walker G, Barbur JL. The variability of normal trichromatic vision and the establishment of the "normal" range. In: *Proceedings of 10th Congress of the International Colour Association*. Granada: International Colour Association. 2005;979–982.
24. Wilk MA, Wilk BM, Langlo CS, Cooper RF, Carroll J. Evaluating outer segment length as a surrogate measure of peak foveal cone density. *Vision Res*. 2017;130:57–66.
25. Dubra A, Harvey Z. Registration of 2D images from fast scanning ophthalmic instruments. In: Fischer B, Dawant B, Lorenz C, eds. *Biomedical Image Registration*. Berlin: Springer-Verlag; 2010:60–71.
26. Wilk MA, McAllister JT, Cooper RF, et al. Relationship between foveal cone specialization and pit morphology in albinism. *Invest Ophthalmol Vis Sci*. 2014;55:4186–4198.
27. Garrioch R, Langlo C, Dubis AM, Cooper RF, Dubra A, Carroll J. Repeatability of in vivo parafoveal cone density and spacing measurements. *Optom Vis Sci*. 2012;89:632–643.
28. Schindelin J, Arganda-Carreras I, Frise E, et al. Fiji: an open-source platform for biological-image analysis. *Nat Methods*. 2012;9:676–682.
29. Buena-Atienza E, Rüther K, Baumann B, et al. De novo intrachromosomal gene conversion from OPN1MW to OPN1LW in the male germline results in Blue Cone Monochromacy. *Sci Rep*. 2016;6:28253.
30. Ueyama H, Muraki-Oda S, Yamade S, et al. Unique haplotype in exon 3 of cone opsin mRNA affects splicing of its precursor, leading to congenital color vision defect. *Biochem Biophys Res Commun*. 2012;424:152–157.
31. Akimitsu N. Messenger RNA surveillance systems monitoring proper translation termination. *J Biochem*. 2008;143:1–8.
32. Michaelides M, Johnson S, Bradshaw K, et al. X-linked cone dysfunction syndrome with myopia and protanopia. *Ophthalmology*. 2005;112:1448–1454.
33. Oyster CW. *The Human Eye: Structure and Function*. Sunderland, MA: Sinauer Associates, Inc.; 1999.
34. Zhang T, Godara P, Blancob ER, et al. Variability in human cone topography assessed by adaptive optics scanning laser ophthalmoscopy. *Am J Ophthalmol*. 2015;160:290–300.
35. Li KY, Tiruveedhula P, Roorda A. Intersubject variability of foveal cone photoreceptor density in relation to eye length. *Invest Ophthalmol Vis Sci*. 2010;51:6858–6867.
36. Tanna P, Kasilian M, Strauss R, et al. Reliability and repeatability of cone density measurements in patients with Stargardt disease and RPGR-associated retinopathy. *Invest Ophthalmol Vis Sci*. 2017;58:3608–3615.
37. Talcott KE, Ratnam K, Sundquist S, et al. Longitudinal study of cone photoreceptors during retinal degeneration and in response to ciliary neurotrophic factor treatment. *Invest Ophthalmol Vis Sci*. 2011;52:2219–2226.
38. Langlo CS, Erker LR, Parker M, et al. Repeatability and longitudinal assessment of foveal cone structure in CNGB3-associated achromatopsia. *Retina*. 2017;37:1956–1966.
39. Morgan JIW, Vergilio GK, Hsu J, Dubra A, Cooper RF. The reliability of cone density measurements in the presence of rods. *Trans Vis Sci Tech*. 2018;7(3):21.
40. Abozaid MA, Langlo CS, Dubis AM, Michaelides M, Tarima S, Carroll J. Reliability and repeatability of cone density

Investigative Ophthalmology & Visual Science

measurements in patients with congenital achromatopsia. *Adv Exp Med Biol*. 2016;854:277–283.

41. Cunefare D, Fang L, Cooper RF, Dubra A, Carroll J, Farsiu S. Open source software for automatic detection of cone photoreceptors in adaptive optics ophthalmoscopy using convolutional neural networks. *Sci Rep*. 2017;7:6620.
42. Nguyen LS, Wilkinson MF, Gecz J. Nonsense-mediated mRNA decay: inter-individual variability and human disease. *Neurosci Biobehav Rev*. 2014;46:175–186.
43. Chang B, Mandal MN, Chavali VR, et al. Age-related retinal degeneration (arrd2) in a novel mouse model due to a nonsense mutation in the Mdm1 gene. *Hum Mol Genet*. 2008; 17:3929–3941.
44. Carroll J, Neitz J, Neitz M. Estimates of L:M cone ratio from ERG flicker photometry and genetics. *J Vis*. 2002;2(8):531–542.
45. Bumsted K, Jasoni C, Szel A, Hendrickson A. Spatial and temporal expressions of cone opsins during monkey retinal development. *J Comp Neurol*. 1997;378:117–134.

Investigative Ophthalmology & Visual Science

Supplementary Materials

Supplementary Table 1. A) Confocal cone density for subjects with X-linked cone dysfunction

Subject	Mutation	Fovea	0.25° T	0.5° T	1° T	2° T	3° T	4° T	5° T	6° T	7° T	8° T	9° T	10° T
JC_0084	**LIAVA**	90,970	76,179	52,855	30,163	12,876	14,318	8,953	7,165	9,516	7,156	5,406	6,148	4,729
MM_0133	**LIAVA**	28,955	12,642	7,547	7,602	7,615	2,146	--	--	--	--	--	--	--
MM_0142	**LIAVA**	52,229	43,299	33,665	23,702	13,240	8,682	2,766	3,544	6,392	5,102	4,158	2,791	--
MM_0144	**LIAVA**	30,585	22,069	22,758	21,700	--	--	--	--	--	--	--	--	--
MM_0145	**LIAVA**	61,666	45,653	31,016	20,294	12,976	9,533	2,228	3,999	3,915	5,481	3,315	3,668	--
MM_0155	**LIAVA**	--	--	--	--	--	--	--	--	--	--	--	--	--
JC_0609	**LIAVA**	19,061	14,086	10,197	7,232	2,232	3,559	3,016	4,237	5,024	2,149	1,157	1,653	2,760
JC_10340	**LVAVA**	--	--	--	--	--	--	--	--	--	--	--	--	--
JC_11437	**LVAVA**	75,229	54,358	40,808	27,224	3,330	--	6,065	5,199	5,830	5,881	3,057	2,958	2,314
JC_11445	**LVAVA**	--	--	--	21,590	12,446	8,056	5,209	5,051	2,810	6,262	3,695	4,183	1,653
MM_0156	**exon 2 insertion**	20,664	23,504	16,083	15,495	11,603	6,879	4,511	5,216	2,149	4,099	5,077	--	--
MM_0157	**exon 2 insertion**	67,566	56,030	37,059	25,736	15,027	10,724	--	--	--	--	--	--	--
MM_0188	**exon 4 splice defect**	44,626	37,156	25,599	16,032	--	--	--	--	--	--	--	--	--

Supplementary Table 1. B) Split-detection cone density for subjects with X-linked cone dysfunction

Subject	Mutation	Fovea	0.25° T	0.5° T	1° T	2° T	3° T	4° T	5° T	6° T	7° T	8° T	9° T	10° T
JC_0084	**LIAVA**	96,625	85,337	68,916	42,140	30,787	17,534	11,417	9,726	7,857	7,444	6,759	4,666	4,852
MM_0133	**LIAVA**	47,391	43,088	32,009	28,876	13,212	8,270	--	--	--	--	--	--	--
MM_0142	**LIAVA**	66,475	58,196	38,504	22,120	12,783	10,853	5,301	4,924	6,453	5,974	3,952	3,433	--
MM_0144	**LIAVA**	59,222	42,916	22,231	17,561	--	--	--	--	--	--	--	--	--
MM_0145	**LIAVA**	55,999	57,797	40,443	18,744	14,632	5,203	5,524	6,543	4,366	3,429	3,179	4,468	--
MM_0155	**LIAVA**	--	--	--	--	--	--	--	--	--	--	--	--	--
JC_0609	**LIAVA**	29,750	24,111	23,842	16,965	10,747	6,399	3,689	1,733	2,314	3,395	3,223	3,889	2,645
JC_10340	**LVAVA**	--	--	--	--	--	--	--	--	--	--	--	--	--
JC_11437	**LVAVA**	--	60,981	51,037	30,668	16,236	9,482	9,798	7,834	7,323	9,679	5,785	7,715	4,071
JC_11445	**LVAVA**	--	--	--	37,891	18,946	13,365	11,111	7,622	5,898	6,060	6,488	6,650	5,192
MM_0156	**exon 2 insertion**	52,938	42,473	30,533	22,123	11,445	7,260	3,876	4,263	3,682	3,252	4,365	--	--
MM_0157	**exon 2 insertion**	62,527	57,070	36,943	25,116	16,933	6,657	--	--	--	--	--	--	--
MM_0188	**exon 4 splice defect**	49,678	42,600	32,610	22,526	4,934	--	--	--	--	--	--	--	--